Transactions of the Korean Nuclear Society Spring Meeting
Jeju, Korea, May 22-23, 2025

Thermal Analysis of Micro-Pillar Structures under Pool Boiling Conditions using Optical Fiber Sensors

Minkyu Park[1], Hyeon Taek Nam[3], Seungro Lee[3], Donghwi Lee[1,2*]
[1]*Graduate school of Mechanical-Aerospace-Electric Convergence Engineering, Jeonbuk National University, 567 Baekje-daero, Deokjin-gu, Jeonju 54896, Republic of Korea*
[2]*Department of Mechanical System Engineering, Jeonbuk National University, 567 Baekje-daero, Deokjin-gu, Jeonju 54896, Republic of Korea*
[3]*Department of Mechanical Engineering, Jeonbuk National University, 567 Baekje-daero, Deokjin-gu, Jeonju 54896, Republic of Korea*
alsrb2954@gmail.com;skagusxor@naver.com;seungrol@jbnu.ac.kr;dlee462@jbnu.ac.kr

***Keywords : Critical Heat Flux(CHF), Optical Fiber Sensors(OFS), Pool boiling, Micro-Pillar structures(MPS)**

1. Introduction

Boiling heat transfer is a crucial mechanism for next-generation cooling systems, leveraging latent heat during phase transitions to achieve high thermal performance. A key parameter in boiling heat transfer is the critical heat flux (CHF) or departure from nucleate boiling (DNB), which defines the maximum heat flux a surface can sustain before transitioning to film boiling. At CHF, a vapor layer forms, drastically increasing surface temperature and reducing heat transfer efficiency. To improve CHF, researchers have explored micro-structured surfaces that enhance fluid rewetting through capillary action. Among these, micro-pillar structures effectively facilitate liquid supply, making them a promising solution for applications such as nuclear reactors.

In pressurized water reactors (PWRs), efficient cooling depends on phase-change heat transfer, where high-pressure water removes heat from nuclear fuel. PWRs typically operate at around 330°C and 15 MPa, but during events like a loss-of-coolant accident (LOCA) or a reactivity-initiated accident (RIA), DNB can occur, forming an insulating vapor layer and rapidly elevating fuel surface temperature. Understanding DNB conditions is critical for reactor safety.

Traditional DNB measurement methods include thermocouples, which provide limited spatial resolution, and infrared cameras, which require optically compatible materials and face challenges in high-pressure environments. This study introduces optical fiber sensors (OFS) for temperature field measurements, offering high spatial and temporal resolution while operating in extreme conditions up to 15 MPa and 750°C. Experiments at atmospheric pressure utilized seven OFS sensors on a 20 × 20 mm² heater, capturing 2D temperature distributions with 1 mm resolution and a 100 Hz sampling rate. The results demonstrate the potential of OFS for high-resolution thermal analysis in boiling systems.

2. Methods and Results

2.1 Experimental setup

Boiling experiment system consists of a boiling chamber, copper block (heater rod), cartridge heater, power supply and data acquisition system. The most attractive point is surface of heater rod. Precisely embedding the optical fiber. To enhance measurement accuracy, grooves were machined into the copper block's surface for fiber placement, but due to machining limitations, they were spaced 750μm apart. This could lower temperature measurement precision, so interpolation was applied to estimate temperatures at unmeasured points. These interpolated values were used to generate a 3D temperature distribution map, improving measurement accuracy through an energy balance equation. The measured temperature data was used to calculate the heat transfer coefficient and heat flux of the surface.

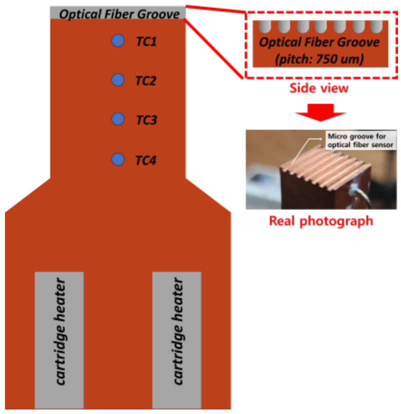

Fig. 1. Schematics of heater rod

2.2 Optical fiber sensor

This study measured high-resolution surface temperature distribution using an optical fiber and a distributed sensor interrogator (LUNA, ODiSI 7100 series). The LUNA ODiSI employs optical frequency domain reflectometry (OFDR) to capture Rayleigh backscattered signals along the fiber. Temperature-induced fiber expansion causes a frequency shift in the backscattered signal, which is used to calculate temperature changes relative to a reference temperature (20℃).

Fig. 2 shows the cross-section of the optical fiber sensor (OFS) inside a SUS capillary tube. The OFS (155µm diameter, including polyimide coating) is housed within a SUS 304 capillary tube (ID: 400µm, OD: 700µm) to maintain a free-strain state, with thermal grease applied to reduce thermal contact resistance. The thermal conductivity of the SUS304 capillary tube is approximately 14–16 W/m·K. A thermal grease (Thermal Grizzly Kryonaut Extreme) with similar thermal conductivity, 14.2 W/m·K, was used to fill the capillary tube. To ensure gap-free filling, thermal grease was introduced either under vacuum conditions or by utilizing capillary action. Due to the complexity of establishing a vacuum environment, the capillary action method was adopted. In this process, the optical fiber sensor was positioned in the groove, after which small amounts of thermal grease were carefully applied around it using a syringe. The thermal grease naturally wicked into the narrow gap via capillary action, progressively filling the interior of the capillary tube. In this experiment, the optical fiber temperature sensor placed inside the capillary tube was assumed to be positioned at the center and the surface temperature analysis was conducted based on this assumption. However, in practice conditions, the optical fiber temperature sensor may be attached to the inner wall of the capillary tube. Calculations show that under a heat flux condition of approximately 10 W/cm², a temperature difference of about 1.5°C can occur compared to the case where the sensor is centrally located. Therefore, future research will consider this effects to calculate the uncertainty in surface temperature measurements.

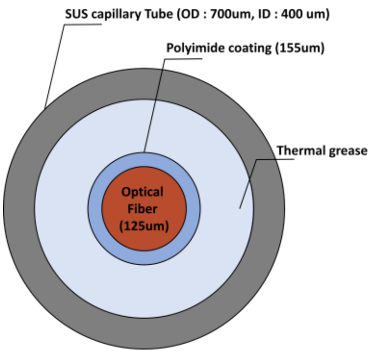

Fig. 2. Schematics of heater rod

2.3 Interpolation of surface temperature

In this study, interpolation was employed to estimate temperatures at locations where direct measurements by the OFS were not possible. These estimated values were then used to construct a three-dimensional (3D) temperature distribution map, enhancing the accuracy of surface temperature assessment. To achieve this 3D mapping, the energy balance equation was applied to interpolate temperatures at unmeasured points, allowing the calculation of temperatures between the optical fiber lines. For instance, the energy balance equation at point ***T₂*** is expressed as follows.

$$(1)\ T = T_{ref} - 1.0862 f_{shift} - 6.1516\times10^{-3} f_{shift}{}^{2} - 3.3691\times10^{-5} f_{shift}{}^{3} - 5.7951\times10^{-8} f_{shift}{}^{4}$$

$$(2)\ q_1 = k\Delta x\frac{T_1-T_2}{\Delta y},\ q_2 = k\Delta y\frac{T_L-T_2}{\Delta x},\quad q_3 = k\Delta x\frac{T_3-T_2}{\Delta y},\quad q_4 = k\Delta y\frac{T_R-T_2}{\Delta y}$$

$$(3)\ \sum \mathrm{q_n} = \mathrm{q_1} + \mathrm{q_2} + \mathrm{q_3} + \mathrm{q_4} = 0$$

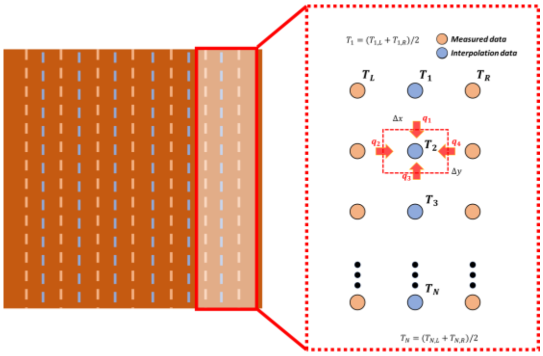

Fig. 3. Interpolation mechanism for Optical Fiber Sensor (OPS) data

The temperature n th point temperature was determined as follows.

$$(4)\ a(T_{n-1}) + b(T_n) + a(T_{n+1}) + c(T_{n,L}) + c(T_{n,R}) = 0$$

$$(5)\ a = \Delta x^2,\ b = -2\Delta x^2 - 2\Delta y^2,\ c = \Delta y^2$$

$$(6)\ \begin{bmatrix} b & a & 0 & 0 & 0 & 0 & 0 \\ a & b & a & 0 & 0 & 0 & 0 \\ 0 & a & b & a & 0 & 0 & 0 \\ & \vdots & & \ddots & & \vdots & \\ 0 & 0 & 0 & a & b & a & 0 \\ 0 & 0 & 0 & 0 & a & b & a \\ 0 & 0 & 0 & 0 & 0 & a & b \end{bmatrix} \begin{bmatrix} T_2 \\ T_3 \\ T_4 \\ \vdots \\ T_{N-3} \\ T_{N-2} \\ T_{N-1} \end{bmatrix} = \begin{bmatrix} -a(T_1) - c(T_{2,L}) - c(T_{2,R}) \\ -c(T_{3,L}) - c(T_{3,R}) \\ -c(T_{4,L}) - c(T_{4,R}) \\ \vdots \\ -c(T_{N-3,L}) - c(T_{N-3,R}) \\ -c(T_{N-2,L}) - c(T_{N-2,R}) \\ -c(T_{N-1,L}) - c(T_{N-1,R}) - a(T_N) \end{bmatrix}$$

The surface temperature distribution, including measured and interpolation data, was contoured using the MATLAB.

3. Conclusions

We mapped the 3D temperature-distribution on the boiling surface. Therefore, the temperature distribution at detailed points can be determined through seven grooves. Compared to a plain surface, the critical heat flux (CHF) on the micro-pillar surface improved by approximately 85%, and the standard temperature deviation was also refined by about 9%. Further experiments will be conducted to obtain more detailed statistical results.

REFERENCES

[1] H. Park, H. Nam, S. Shin, N. Lee, H. Cho, D. Lee, Temperature-dependent wicking dynamics and its effects on critical heat flux on micropillar structures in pool boiling heat transfer, International Communications in Heat and Mass Transfer 146 (2023) 106887

[2] A. Luna, T. A. Moreira, M. Corradini, M. Anderson, Fiber optic sensors for monitering elongation, swelling, and temperature in a simulated nuclear fuel cladding, IEEE Sensors Council (2025) 1558-1748

[3] H. Park, H. Nam, S. Shin, N. Lee, H. Cho, D. Lee, Enhancing pool boiling heat transfer performance via deposition of nanoparticles with different sizes on micropillar surfaces, International Communications in Heat and Mass Transfer 160 (2025) 108282

[4] H. Nam, H. Cho, S. Lee, D. Lee, Two-phase particle image velocimetry visualization of rewetting flow on the micropillar interfacial surface, ACS Applied Materials & Interfaces 2024, 16, 34313-34325